nature portfolio

https://doi.org/10.1038/s41558-022-01344-2

Supplementary information

Observed influence of anthropogenic climate change on tropical cyclone heavy rainfall

In the format provided by the authors and unedited

Supplementary Information for

Observed influence of anthropogenic climate change on tropical cyclone heavy rainfall

[1)] *Nobuyuki Utsumi and [2,3,4)] *Hyungjun Kim

1) Nagamori Institute of Actuators, Kyoto University of Advanced Science, Kyoto, Japan

2) Moon Soul Graduate School of Future Strategy, Korea Advanced Institute of Science and Technology, Daejeon, Korea

3) Department of Civil and Environmental Engineering, Korea Advanced Institute of Science and Technology, Daejeon, Korea

4) Institute of Industrial Science, The University of Tokyo, Tokyo, Japan

Tropical Cyclone Existence Frequency

Figures S1a and S1b compare the TC existence frequency for the observation and historical simulation. The simulation well reproduces the general spatial pattern of the TC existence frequency in the WNP region. The bimodal peaks of the existence frequency around the east and west of the Philippines is represented by the simulation with a slight overestimation in the tropical Pacific Ocean.

Figure S1c shows the seasonality of the expected number of TCs in the western North Pacific. The simulated seasonality is within the range of the observed uncertainty, although the seasonality of the TC frequency in the simulation shows a peak one-month later compared to that in the observation.

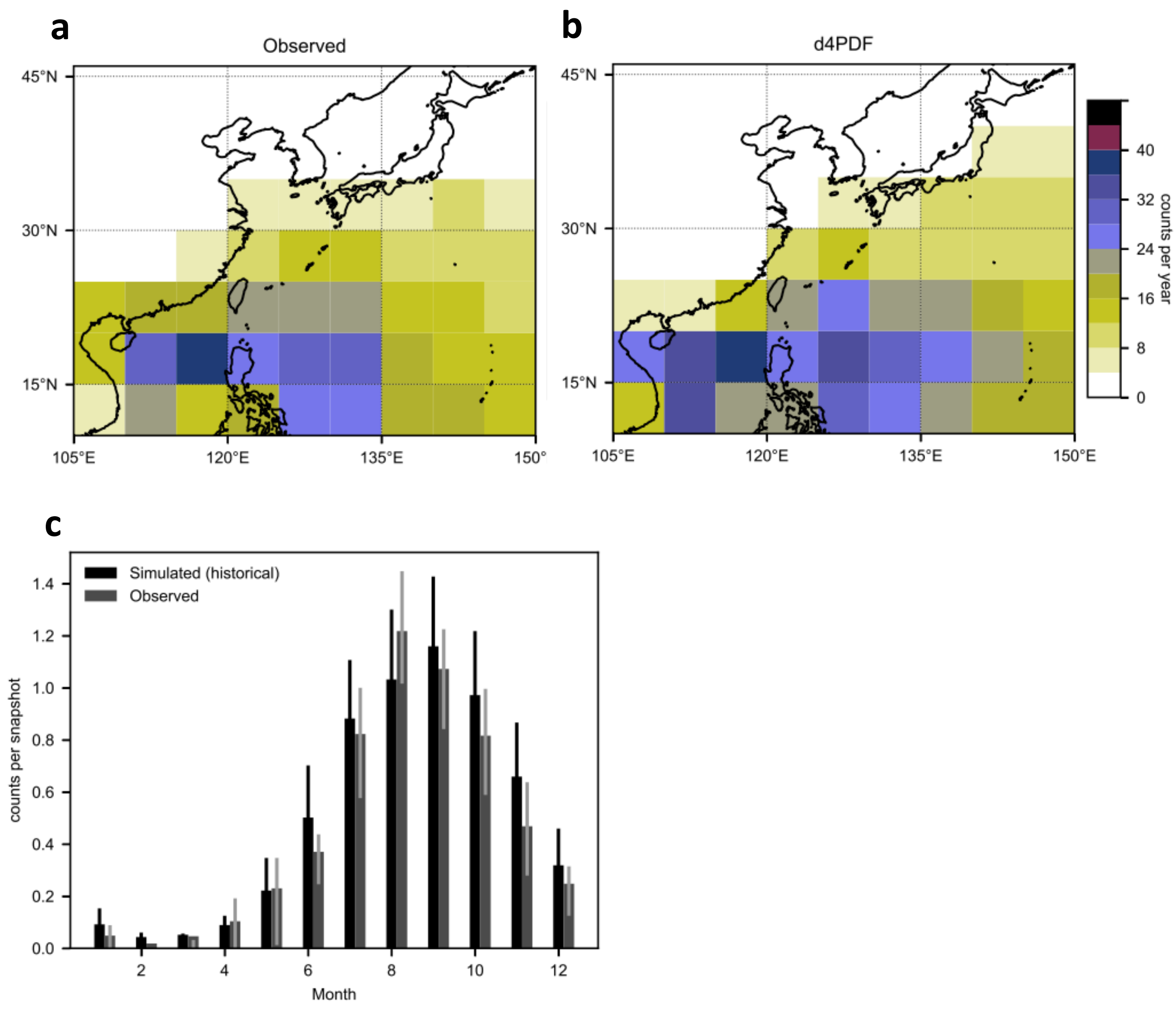

Figure S1. Tropical cyclone existence frequency. a) Observation and b) ensemble average of historical runs. Units are counts per year. The analyses are performed at 5° × 5° grid boxes based on 6-hourly time step data. Bar plot depicting c) Seasonality of the average number of TCs per snapshot. Error bar represents the range of 5 and 95 percentiles. All figures are for 1980–2010.

Bias correction of tropical cyclone rainfall intensity

Figure S2 shows the cumulative distribution function of TC rainfall intensity for observation and d4PDF simulation. The d4PDF simulation (red curve in Figure S2a) reproduces the overall shape of the observed TC rainfall intensity (black curve in Figure S2a) but there is some bias in the higher percentile ranges (Figure S2b). To minimize the simulation bias, we employed a bias correction method at each 10° latitude band of the target region. The correction function is estimated by fitting an exponential function to the quantile-quantile plot of observed and simulated TC rainfall intensity (Figure S2c). The same correction function is applied to both historical and natural experiments. We confirmed that the bias correction does not change the conclusion of the current study (see the next section). Similar statistical bias corrections were employed by previous studies for the analysis of tropical cyclones[9].

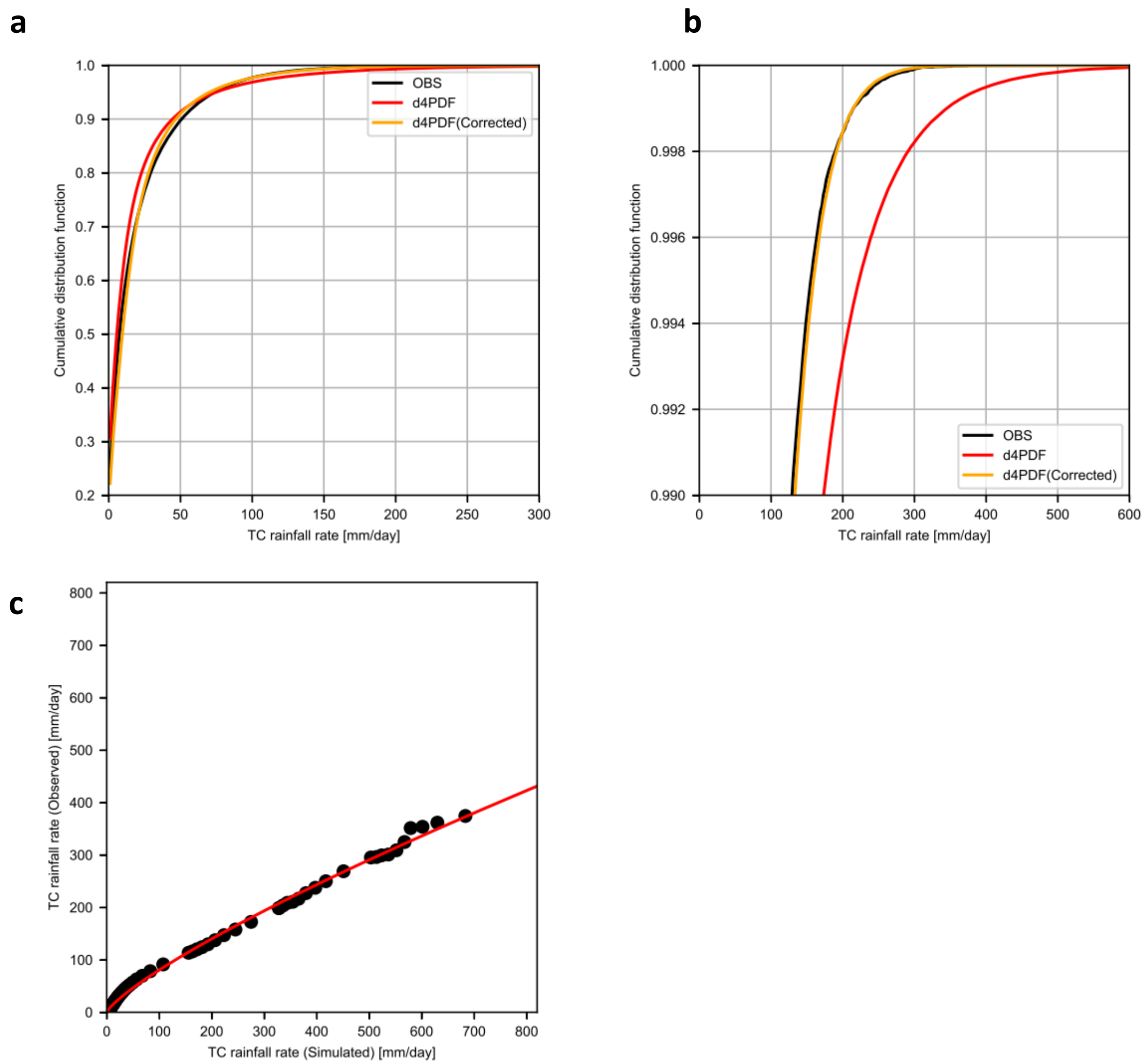

Figure S2 Cumulative distribution function (CDF) of tropical cyclone rainfall intensity. a) Overall CDF. b) same as (a) but focused on the highest percentile range. c) Example of the quantile-quantile plot of TC rainfall intensity for observation and simulation (for 20°N - 30°N). Fitted exponential curve is shown by the red line.

Robustness of the fingerprint analysis to the bias correction

The time series of the detection signal estimated from the raw data (i.e., without bias correction) (Figure S3a) is almost identical to that estimated with bias correction (main manuscript Figure 4a) and their difference is sufficiently small (Figure S3b). Note that the vertical axes in Figures S3a and S3b differ by two orders of magnitude. The difference is mainly attributable to the fitting residuals of the bias correction curve (Figure S2c). Since the finger print $\vec{f}$ used to calculate the detection signal is obtained from the simulated data (see the Methods section in the main manuscript), such difference due to the bias correction propagates to the detection signal for the observation, but the impact is negligible (red line of Figure S3b). As a result, the linear trends of the uncorrected (Figure S3c) and bias-corrected (Figure 4b) detection signals are almost identical. This indicates that the conclusions of the current study are robust for the bias correction applied to the d4PDF simulation data.

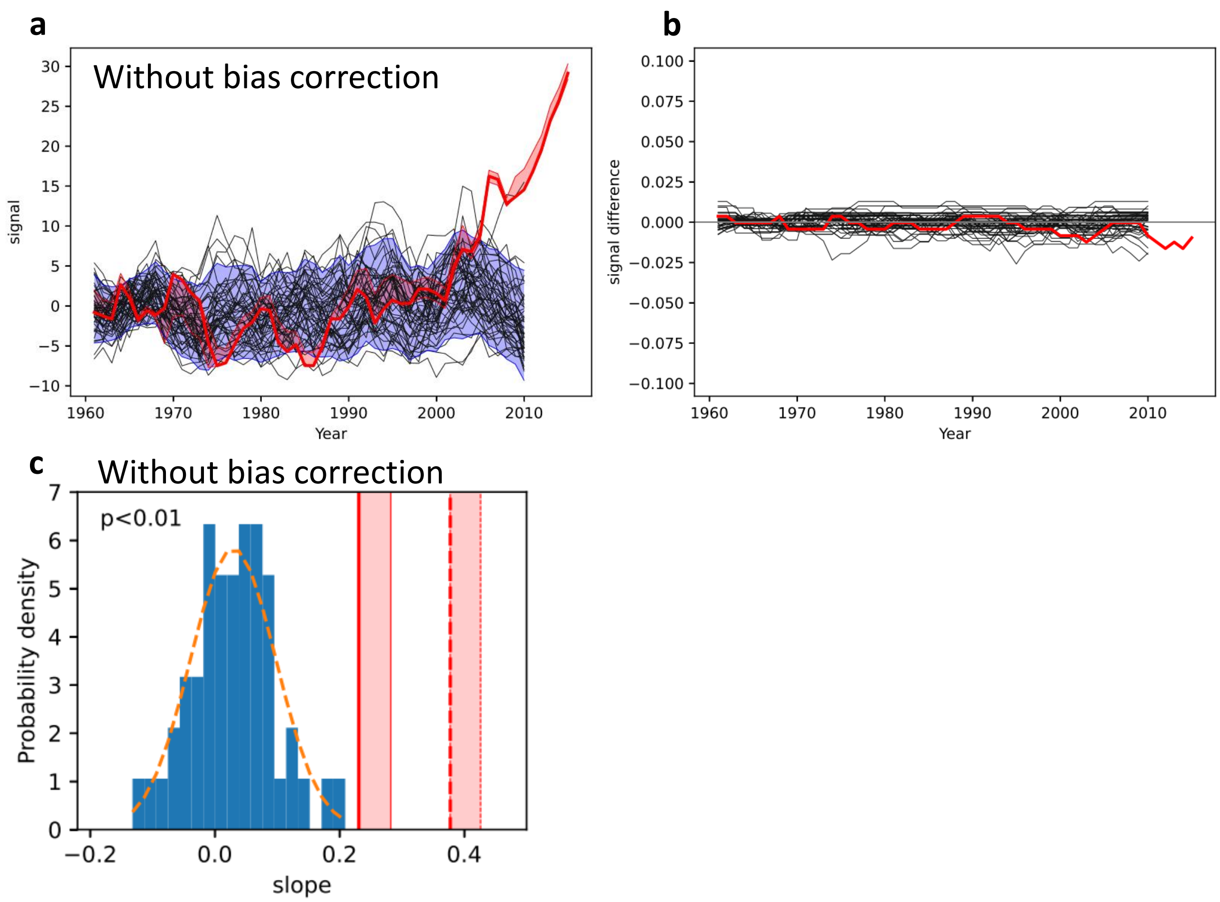

Figure S3 Finger print analysis without bias correction. a) Same as Figure 4a but without bias correction. b) Difference between the uncorrected and bias corrected detection signals (bias corrected – uncorrected). c) Same as Figure 4b but without bias correction.

Tropical cyclone heavy rainfall frequency

Figure S4 shows the observed and dPDF simulated historical frequency of TC heavy rainfall. The d4PDF ensemble average generally reproduces the spatial pattern of the observed TC heavy rainfall frequency, although the simulation shows a smoother gradient due to the large ensemble size. The figure also indicates that the observed frequency at most of the land pixels are in the range of d4PDF ensemble spread (in between 10 – 90 percentiles of the ensemble members), which means that the d4PDF simulation successfully captures the observed pattern within the ensemble envelope.

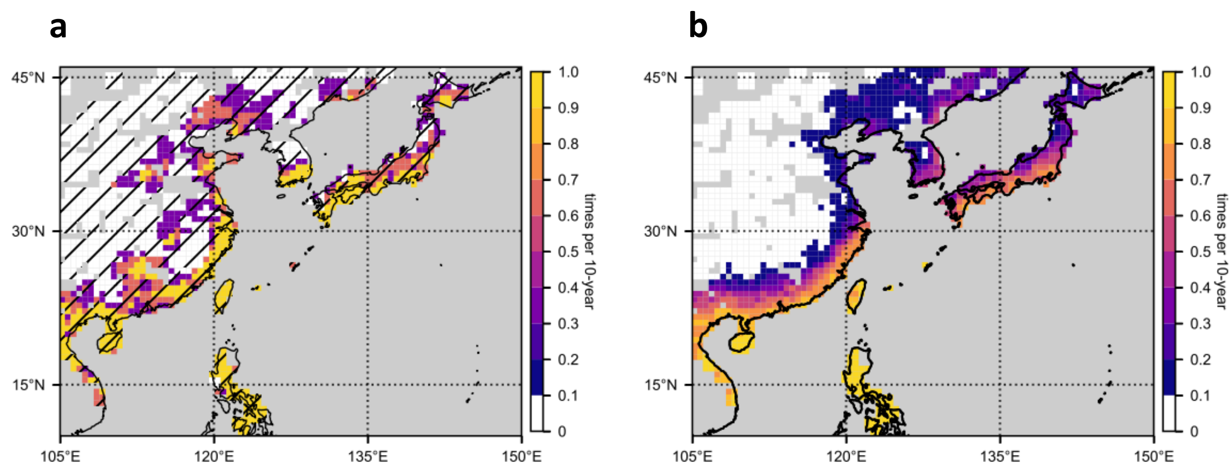

Figure S4 Frequency of TC heavy rainfall (times/10-year). a) Observation and b) ensemble average of d4PDF historical experiment (ensemble 1 – 20, after the bias correction applied) for 1980 – 2010. Observation pixels that are in the range of d4PDF ensemble spread (in between 10 – 90 percentiles) are hatched.

Pixel selections of the observational dataset

We used the gauge-based 0.5° resolution gridded daily precipitation dataset, Asian Precipitation - Highly-Resolved Observational Data Integration Towards Evaluation of Water Resources (APHRODITE) for monsoon Asia V1101[28] (and its extension V1101EX_R1), as the observational dataset. APHRODITE provides daily rain gauge information at each 0.5° grid box every day. At each 0.5° grid box, we calculated the number of days where at least one rain gauge is available at the grid box ("with-gauge-days"). This data is then projected onto the analysis resolution of ~60km by simply checking the corresponding 0.5° dataset at each ~60km grid box center location. Figure S5a shows the fractional number of with-gauge-days at each analysis grid box (~60km resolution) for 1961 – 2010. In order to keep the balance between the long-term reliability of the observation and spatial coverage, the grid boxes of with-gauge-days ≥ 90% (green pixels in Figure S5b) and their adjacent grid boxes (blue pixels in Figure S5b) are used for the analyses. It shows that the grid boxes with sufficient rain gauge observations are well distributed in the target domain, particularly in the tropical cyclone-affected coastal regions. In addition, it is confirmed from Figure S5c that the number of with-gauge-days is almost evenly distributed over the analysis period for the green pixels shown in Figure S5b.

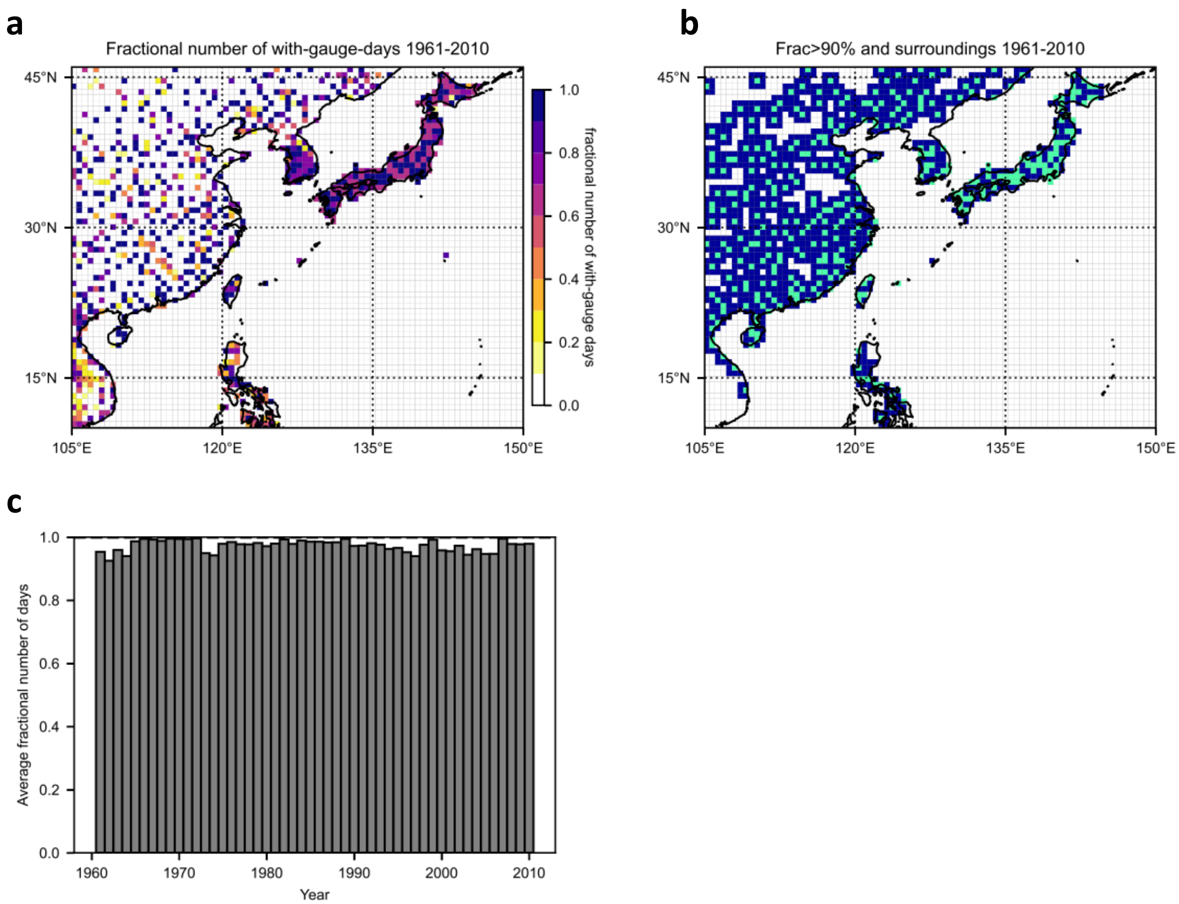

Figure S5 Rain gauge information. a) Fractional number of days where at least one rain gauge is contained at the grid box (with-gauge-days) during 1961 – 2010. b) grid boxes with the fractional number of with-gauge-days ≥90% (green) and their adjacent grid boxes (blue). c) Time series of the average fractional number of with-gauge-days for the green pixels of panel (b).

Sensitivity to the choice of comparison periods.

This study exploits combined use of the d4PDF large ensemble simulation and the APRODITE observation data. We used 1985 as partition line for Figure 1a since it divides the overlapped period (1961 – 2010) of the two data used in this study. In order to see the sensitivity of Figure 1a to the choice of comparison periods (1961 – 1985 to 1986 – 2015), the same analysis was conducted for the different choices of partition year (1985 $\pm$3; Figure S6). Both cases show almost the same pattern as Figure 1a, indicating that the spatial pattern of the changes in TC heavy rainfall frequency is robust to the a few years difference in comparison periods.

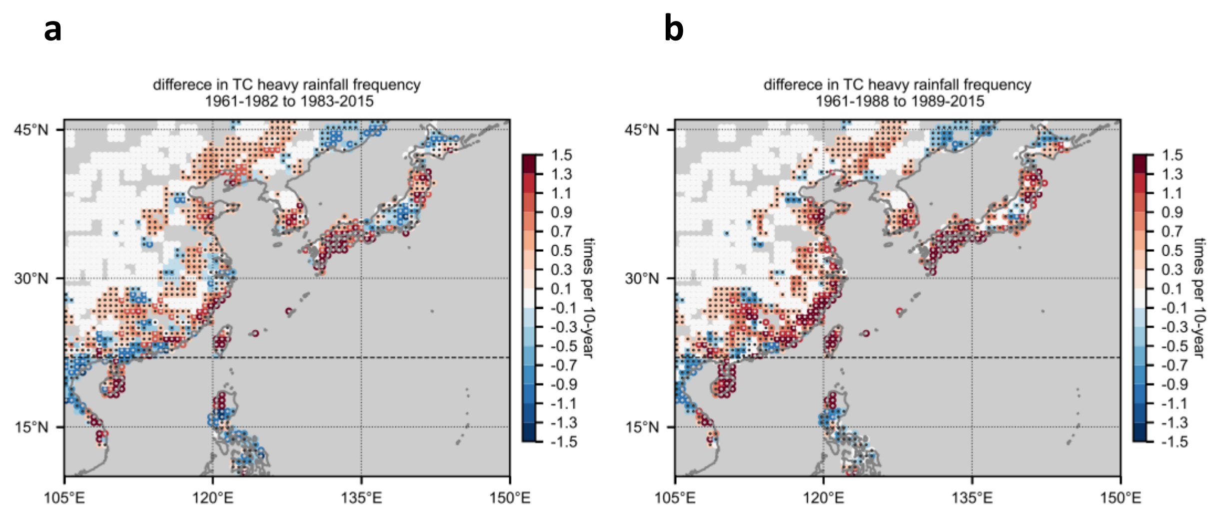

Figure S6 Same as Figure 1a but the comparisons are for a) 1961 – 1982 to 1983 – 2015 and b) 1961 – 1988 to 1989 – 2015. Units are in times/10-year.

Latitude of Lifetime Maximum Intensity

Figure S7 shows the latitudes where the TCs attain their lifetime maximum, which were measured by the central pressure deficit. A poleward shift in the TC lifetime maximum location was found. This implies that the mid-latitude regions have stronger TCs in the historical run. This result suggests that more TCs sustain their intensity until they reach middle latitudes, which contributes to the increased number of TC counts in these latitudes.

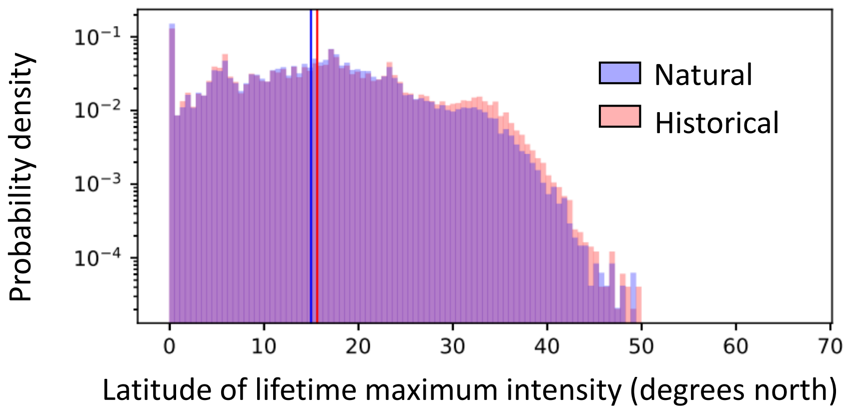

Figure S7 Latitude of TC lifetime maximum intensity. TC intensity is measured by central pressure deficit (hPa). Blue and red bars are for natural and historical d4PDF runs, respectively. Data from 50 ensemble members for 1990–2010 are used. Blue and red vertical solid lines show the averages of the natural and historical experiments, respectively.

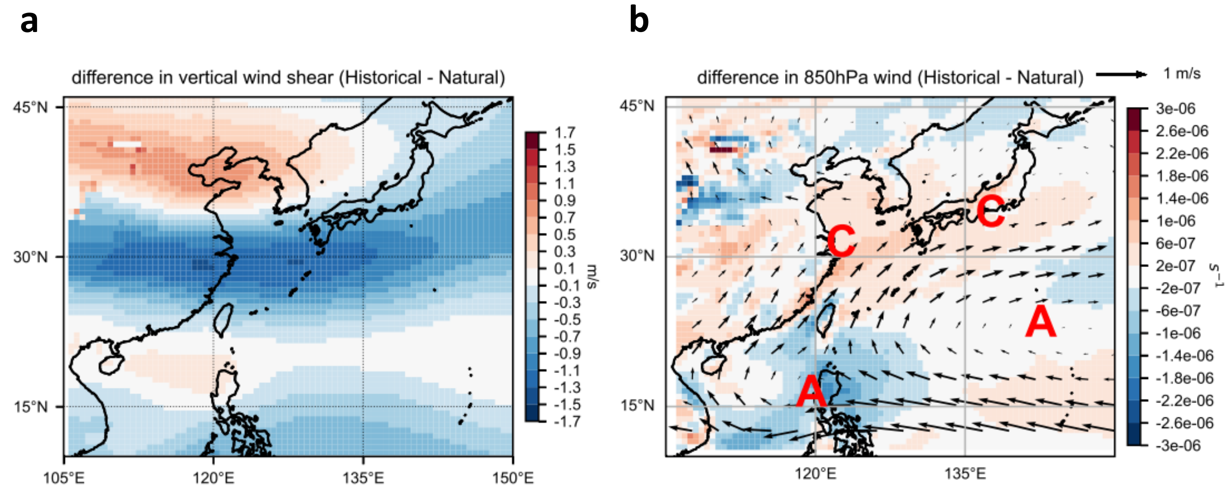

Figure S8 Differences in background environment between natural and historical simulations. a) Difference of vertical wind shear (m/s) (300hPa – 850hPa). b) Difference of the 850hPa wind (m s^{-1}) (vector) and 850hPa vorticity (s^{-1}) (colored-contour). Red "C" and "A" letters show the positions of cyclonic and anticyclonic anomaly of low-level flow, respectively. Differences (historical – natural) are calculated from the average of 1–50 ensemble members for May–October during 1990–2010.

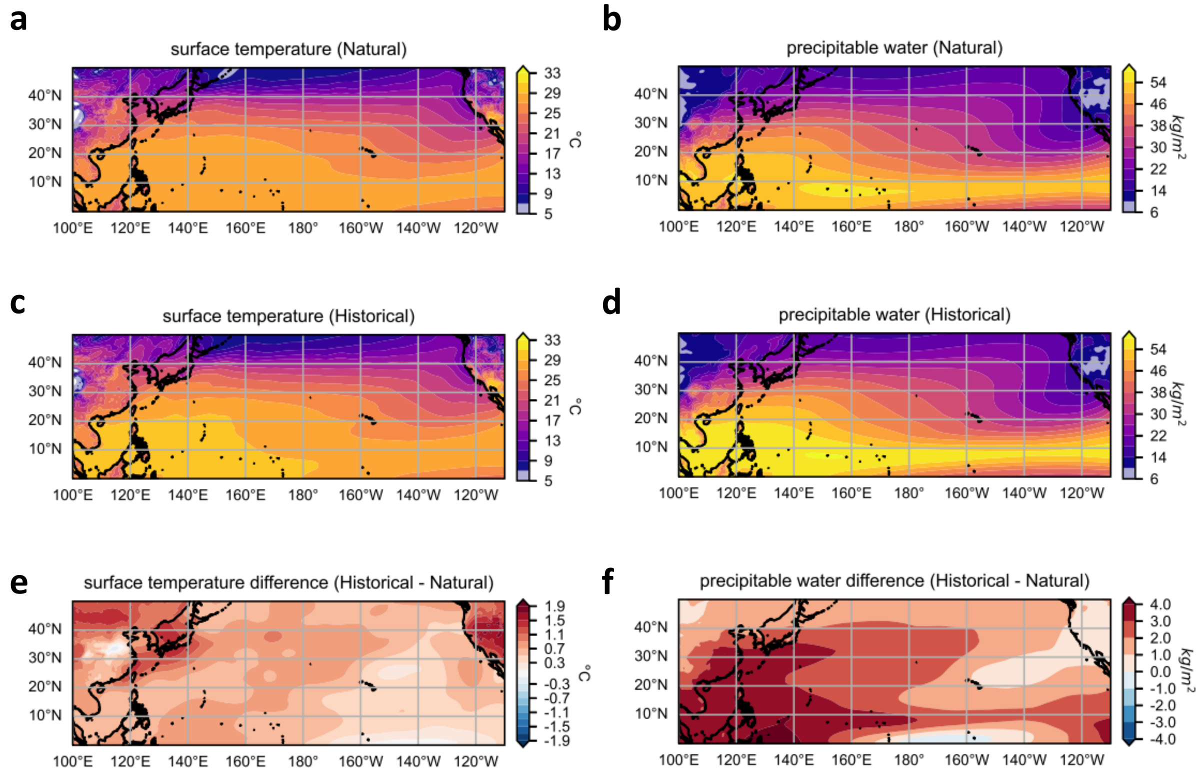

Figure S9 Comparisons of surface temperature and precipitable water between natural and historical runs. a), c), e) Surface temperature and b), d), f) precipitable water for a), b) natural runs, c), d) historical runs, and e), f) difference between natural and historical runs (historical – natural). All figures are from the average of the 1 – 50 ensemble members for May–October during 1990–2010.

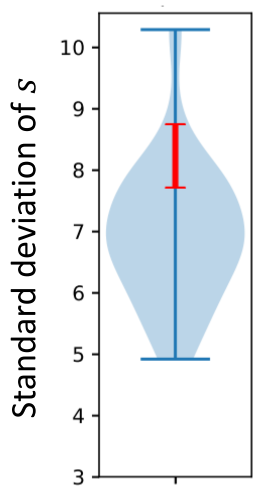

Figure S10 Year-to-year standard deviations of the detection signals. Violin plot shows the distribution of the standard deviation for natural run ensemble members. Blue horizontal lines are the minimum and maximum. Red vertical line shows the range of the detrended detection signal of the observation based on four different agencies for the TC best track dataset.